Available online at www.sciencedirect.com
ScienceDirect
Journal of the European Ceramic Society 27 (2007) 4675–4683
www.elsevier.com/locate/jeurceramsoc

Design of 7 wt.% Y_2O_3–ZrO_2/mullite plasma-sprayed composite coatings for increased creep resistance

Elizabeth Withey [a], Christopher Petorak [a], Rodney Trice [a,*], Graeme Dickinson [b], Thomas Taylor [b]

[a] *School of Materials Engineering, Purdue University, West Lafayette, IN 47907-2044, United States*
[b] *Praxair Surface Technologies Inc., Indianapolis, IN 46224, United States*

Received 15 October 2006; received in revised form 29 January 2007; accepted 23 February 2007
Available online 18 April 2007

Abstract

Plasma-sprayed stand-alone coatings of 7 wt.% Y_2O_3–ZrO_2 (YSZ), nominally 74 wt.% Al_2O_3–26 wt.% SiO_2 mullite, and a 46:54 volume ratio composite of YSZ to mullite were examined using X-ray diffraction, dilatometry, and compression creep. X-ray diffraction and dilatometer results showed that the as-sprayed predominantly amorphous mullite crystallized at 970 °C. Creep tests were conducted on all three coating types in the as-sprayed condition at stresses from 40 to 80 MPa and temperatures of 1000–1200 °C. The primary deformation mechanism in coatings made from all three materials was stress-assisted densification of the porous coating. While the creep behavior of YSZ/mullite composite specimens was between that of pure YSZ and pure mullite specimens for all combinations of temperature and stress tested, the creep response of the composite was more similar to that of pure mullite for all cases tested, consistent with mullite being the continuous phase in the composite.

Keywords: Mechanical properties; Creep; Mullite; ZrO_2; Coatings

1. Introduction

Thermal barrier coatings (TBCs) are commonly used to protect metallic components of turbine engines that could melt or oxidize at high service temperatures.[1–9] Many TBC systems consist of a ceramic topcoat plasma-sprayed onto an intermetallic bond coat attached to a superalloy substrate. yttria-stabilized zirconia (7 wt.% Y_2O_3–ZrO_2 or YSZ) is commonly used as the ceramic topcoat in these systems because of its high melting temperature (~2700 °C) and low thermal conductivity (~2 W/m/K).[1] For example, a 200 μm thick coating of YSZ can decrease the surface temperature of a metallic component ~200 °C.[2,5] This insulative layer can increase the efficiency and/or lifetime of key turbine engine components by affording higher operating temperatures and/or by decreasing the temperature of metallic engine components.[6,7]

In the as-sprayed state, YSZ coatings have a lamellar microstructure containing columnar grains perpendicular to the substrate along with intralamellar cracks and interlamellar pores.[3,6,7] Upon engine start-up, the combustion of the fuel exposes the top surface of the YSZ coating to temperatures of 1200–1300 °C.[4,10] Due to the low thermal conductivity and transient heating of the coating, a thermal gradient is established through the thickness of the YSZ coating which results in a biaxial compressive stress gradient through its thickness.[8,11] Kokini and others have shown that plasma-sprayed coatings almost immediately begin to relax this stress.[11–16] On engine cooling, a tensile stress gradient through the thickness of the coating develops in proportion to the amount of in-service relaxation that occurred. This tensile gradient can lead to through thickness cracks in the coating, which can eventually cause spallation and failure of the coating.[11]

If the amount of coating relaxation during initial heating is reduced, the magnitude of the tensile stress in the coating during cooling should decrease. In the following work, a two-phase composite coating was designed, fabricated, and evaluated with the overall purpose of reducing the creep response in compression. A blend of YSZ and mullite phases was chosen for this new topcoat. The thermal properties of both materials are compared in Table 1.[17] Mullite was chosen for its excellent creep

* Corresponding author.
E-mail address: rtrice@purdue.edu (R. Trice).

0955-2219/$ – see front matter © 2007 Elsevier Ltd. All rights reserved.
doi:10.1016/j.jeurceramsoc.2007.02.214

Table 1
Comparison of the coefficient of thermal expansion (CTE), melting temperature, and thermal conductivity (k_{th}) of YSZ and mullite[17]

Material	CTE ($^\circ C^{-1}$) ($\times 10^{-6}$)	Melting temperature ($^\circ$C)	k_{th}[a] at 1000 °C (W/m/K)
YSZ	10–11	~2700	2.3
Mullite	5.3	1828	3.7

[a] Based on dense specimens.

resistance.[18,19] Kokini et al.[15] predicted using analytical models that mullite did relax less than YSZ at high temperatures. In their models they showed that coatings of mullite did not form through thickness cracks on cooling, unlike the YSZ coatings tested under the same conditions. Yoon and Chen[20] have shown that rigid mullite inclusions in a tetragonal YSZ matrix decreased the creep rate of zirconia/mullite composites, and that this effect increased with the mullite up to 50%. However, mullite has a lower coefficient of thermal expansion (CTE) and a higher thermal conductivity than YSZ, which could be detrimental to the new coating design by increasing the CTE mismatch between coating and substrate and reduce its ability to insulate the underlying metallic structure.

In this study, a composite thermal barrier coating made from a combination of YSZ and mullite was investigated. Powders of each phase were mechanically mixed together, sprayed and stand-alone coatings were formed. These coatings were compression creep tested at temperatures of 1000 through 1200 °C and stresses of 40–80 MPa. The goal was to design a coating system that crept less in compression than the industry standard 7 wt.% Y_2O_3–ZrO_2 thermal barrier coating.

2. Experimental procedures

2.1. Sample preparation

Cylindrical tubes of YSZ, mullite, and YSZ/mullite composite were fabricated by air-plasma spraying spray-dried 7 wt.% Y_2O_3–ZrO_2 (~82 μm), fused and crushed mullite (~100 μm), and a mechanically mixed combination of the two powders onto a 12.7 mm diameter hollow aluminum rod (Praxair Surface Technologies (PST), Indianapolis, IN). YSZ coatings were sprayed using a PST 1108 torch, and a Metco F4 torch for the mullite and composite coatings. Coatings of each material type were sectioned into 15–20 mm tall specimens using the procedure specified by Dickinson et al.[12] The two faces of each specimen were machined parallel on a lathe via a diamond tool. The thickness of the coatings was ~650 μm, with the inner diameter set at 12.7 mm by the aluminum substrate. The aluminum substrate was removed using a 40% aqueous HCl solution, after which specimens were ultrasonically cleaned in deionized water.

2.2. Physical characterization

2.2.1. SEM characterization

Micrographs of the coatings were taken with a Hitachi S4800 FESEM using an accelerating voltage of 5 keV. To determine the fine grain features in each plasma-sprayed coating, samples of each coating type were fractured by hand and viewed in cross-section. The volume fraction of the YSZ and mullite phases was calculated using a manual point-count method on SEM micrographs of the polished cross-sections of as-sprayed specimens.[21]

2.2.2. Density measurements

The Archimedes' method[22] was used to determine the bulk density of each cylindrical coating after ultrasonic cleaning. The total porosity of the coatings was calculated using theoretical densities of 3.18 and 6.08 g/cm^3 for mullite and YSZ, respectively.[23,24] The theoretical density of the composite coatings was determined using an upper bound rule-of-mixtures approach, utilizing the theoretical densities of YSZ and mullite and the previously calculated volume fractions of YSZ and mullite.

2.2.3. Phase analysis

X-ray diffraction[1] (XRD) was performed on pulverized mullite specimens over 2θ values of 20–80° in the as-sprayed condition and after a 50 h heat treatment at 1400 °C in air. A scan rate of 10°/min with a step size of 0.05° was used.

2.2.4. Thermal expansion measurements

The average in-plane coefficient of thermal expansion for each coating type was determined by testing three or more cylindrical specimens using a dilatometer (Orton Dilatometer Model 2016STD). Each specimen was heated at 5 °C/min to 1200 °C while simultaneously recording the change in height as a function of temperature. The CTE of each mullite and composite specimen was determined between 200 and 550 °C, and between 200 and 800 °C for YSZ specimens. These temperature ranges corresponded to the most linear behavior in the dilatometer data. The predicted CTE of the composite coating was calculated employing a rule of mixtures using the measured volume fractions of YSZ and mullite.

2.3. Creep testing

2.3.1. Creep testing procedure

The in-plane creep behavior of YSZ, mullite, and the composite stand-alone cylindrical coatings was measured using a servo-hydraulic load frame (MTS 810) outfitted with hydraulic collet grips (MTS 646) and an alignment fixture (MTS 609), a 100 kN force transducer, SiC pushrods, and a high-temperature furnace (Applied Test Systems, Inc.). Strain was measured using a high-temperature extensometer (MTS 632.70H-01) with a res-

[1] Siemens Kristalloflex Diffraktometer 500 using Cu Kα radiation.

Table 2
Average bulk density, total porosity, and thickness of as-sprayed coatings of coating type

Material	Bulk density (g/cm^3)	Theoretical density (g/cm^3)	Total porosity (%)	Thickness (μm)
YSZ	5.2 ± 0.2	6.08	14.5 ± 3.0	650
Composite	3.6 ± 0.1	4.51[a]	19.8 ± 2.0	670
Mullite	2.5 ± 0.1	3.18	21.4 ± 3.0	630

[a] Calculated using rule of mixtures based on 46 vol.% YSZ/54 vol.% mullite.

olution of ±1 μm. The extensometer consisted of an alumina pushrod that extended vertically through the center of the lower SiC pushrod platen and the hollow stand-alone coating. Strain was determined by measuring the displacement between the upper stationary SiC platen and the cantilever supporting the alumina pushrod.[13] Alignment of the load frame was adjusted prior to testing the coatings to ensure that load was distributed equally around the circumference of the sample. Alignment was achieved by elastically loading a cylindrical aluminum specimen that had four strain gages[2] positioned 90° from each other on the outside surface. The alignment fixture was then adjusted until identical strain readings were obtained from the same strain gage as it was rotated clockwise 360°. For a 15 mm tall sample, it was possible to measure strains to ±0.03%.

Creep samples were heated at 10 °C/min to 1000, 1100, or 1200 °C and allowed to equilibrate for 15 min. Specimens were then loaded in compression at 20 N/s to stresses of 40, 60, or 80 MPa and held for 5 h. While past researchers have crept YSZ coatings for as long as 70 h using similar cylindrical geometries,[25] our initial creep investigations of mullite and YSZ/mullite composite coatings were intentionally kept short so that more testing conditions and replicates could be evaluated. Further studies would be needed to isolate the long-term creep behavior of mullite and YSZ/mullite coatings.

Sample variability was determined by testing three of each coating type at 40 MPa and 1000 and 1200 °C. This variability was established to be ±0.09 and ±0.03% strain for YSZ and mullite coatings, respectively, independent of the test temperature. For composite coatings the variability was ±0.05% strain at 1000 °C and ±0.15% strain at 1200 °C. Small variations in the initial elastic strain across materials and individual coatings of the same material were attributed to differences in the porosity of each specimen. Thus, before comparing the plastic creep behavior of each stand-alone coating the elastic strain was subtracted.

2.3.2. Characterization of creep behavior

Within the limited time frame of the creep test, each sample demonstrated an apparent steady-state strain rate that was calculated from the slope of the linear portion of the creep data between 10,000 and 17,000 s. Comparison of these rates for each coating type provided a basis for evaluating differences in coating response to combinations of stress and temperature. These apparent steady-state stress rates, $\dot{\varepsilon}_{ss}$ were also used to determine the activation energy for each coating type according to:

$$\dot{\varepsilon}_{ss} = A\sigma^n \, e^{-Q/RT} \quad (1)$$

where A is the material dependent constant, σ the applied stress, n the stress exponent, Q the creep activation energy in kJ/mol, R the universal gas constant (8.314 J/mol/K), and T is the test temperature in Kelvin.[26] For specimens that failed during the creep test, the steady-state strain rate was calculated from the linear portions of the data prior to the tertiary creep regime.

3. Results and discussion

3.1. As-sprayed microstructure

The average amount of mullite in a composite coating was calculated to be 54 ± 4 vol.% from seven images taken randomly throughout a typical composite specimen. An example of an image analyzed is shown in Fig. 1. The calculated theoretical density of the YSZ/mullite composite based on these measurements is presented in Table 2 along with the theoretical densities of YSZ and mullite and the average bulk densities and total porosities of each type of coating. Total porosity was highest in the mullite and YSZ/mullite composite specimens.

Fracture surfaces of as-sprayed coatings revealed a stacked lamellar pattern with interlamellar pores and intralamellar cracks in YSZ coatings and in the YSZ regions of the composite coatings (Fig. 2). Both the pure YSZ and composite coatings also showed columnar YSZ grains perpendicular to the lamellae length (Fig. 2a and b). The fracture surface of the mullite speci-

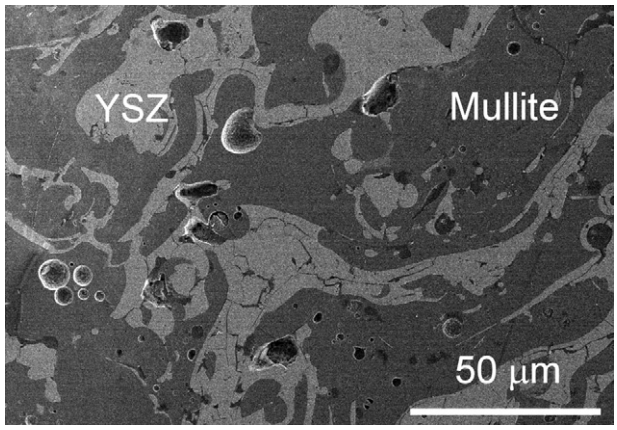

Fig. 1. Back-scatter SEM micrograph of an as-sprayed composite coating taken at a random location in the composite coating showing a 46:54 volume ratio of YSZ (white) to mullite (grey).

[2] Vishay Measurements Group, Raleigh, NC.

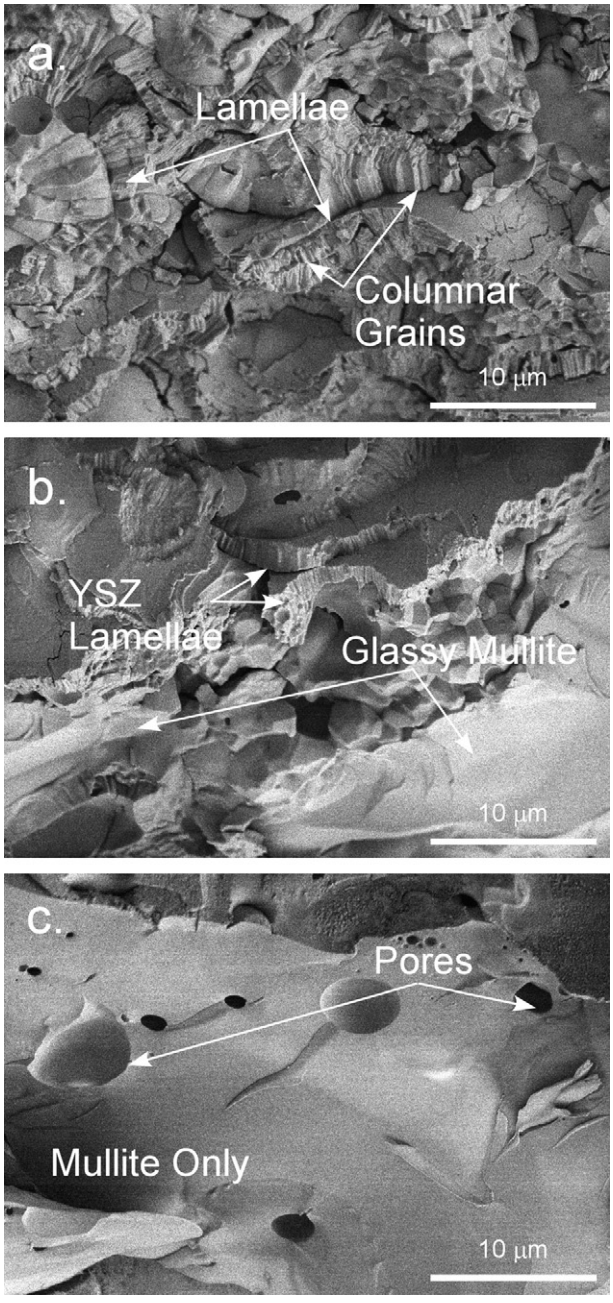

Fig. 2. SEM micrographs of fracture surfaces of: (a) YSZ, (b) YSZ/mullite composite, and (c) mullite as-sprayed coatings. The YSZ phase appears as lamella structures, with columnar grains apparent. The mullite phase appears glassy. Porosity is apparent in both phases.

men appeared to be glassy (Fig. 2c), as has also been observed by Ramaswamy et al.[2] This result was confirmed using XRD (see Fig. 3). The as-sprayed mullite specimens showed an amorphous background; however, 50 h heat-treated specimens showed well-defined peaks. Distinct regions of crystalline YSZ and glassy mullite were observed in the composite coating (Fig. 2b).

3.2. Coefficient of thermal expansion

As shown in Fig. 4, all three coatings exhibited an approximately linear thermal expansion upon heating. For YSZ, this

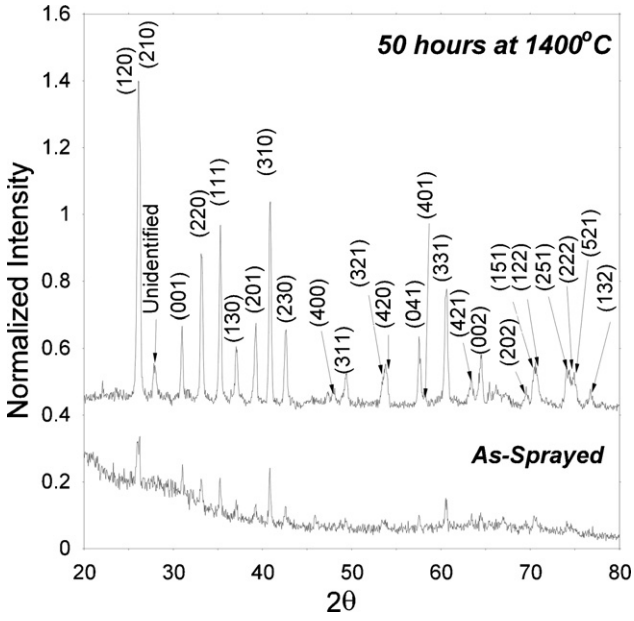

Fig. 3. XRD analysis of as-sprayed (bottom) and heat-treated mullite specimens (50 h at 1400 °C) (top) showing the glassy nature of mullite in the as-sprayed condition and subsequent crystallization during heat treatment.

behavior was consistent across the entire temperature range, whereas mullite and composite specimens showed dramatic shrinkage at ~970 °C. This shrinkage was due to the crystallization of amorphous mullite in these coatings. To further verify that the coatings were crystallizing, the same mullite and composites samples were tested a second time; no discontinuous change in height at ~970 °C was observed.

The measured values of the CTEs of each type of coating have been recorded in Table 3. The measured CTE for YSZ agrees with previously published values by Thurn et al.[27] A value of $4.0 \pm 0.2 \times 10^{-6}\,^{\circ}C^{-1}$ was measured for the mullite specimens. However, data from Lee et al. give a CTE of $5.4 \times 10^{-6}\,^{\circ}C^{-1}$

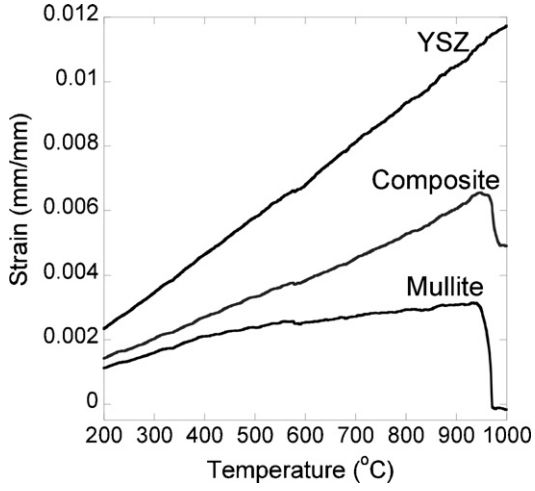

Fig. 4. Linear change vs. temperature for YSZ, mullite, and composite specimens. The YSZ shows linear behavior over the entire temperature range, while mullite and composite specimens only show linear behavior over a limited range of temperatures. A drastic increase in shrinkage of the coatings containing mullite occurs at 970 °C associated with the crystallization of mullite.

Table 3
Measured coefficients of thermal expansion for YSZ, composite, and mullite specimens

Material	Average CTE ($^{\circ}C^{-1}$) ($\times 10^{-6}$)
YSZ	11.0 ± 0.6
Composite	6.4 ± 0.5
Mullite	4.0 ± 0.2

for plasma-sprayed mullite.[28] This discrepancy could be due to differences in the ratio of Al_2O_3 to SiO_2 in the mullites measured.[29] The measured CTE value for the YSZ/mullite composite was $6.4 \pm 0.5 \times 10^{-6}\,^{\circ}C^{-1}$. The calculated CTE value for the YSZ/mullite composite sample based on an upper bound rule of mixtures and the experimental values collected for pure mullite and YSZ coatings was $7.2 \times 10^{-6}\,^{\circ}C^{-1}$, which is close agreement with the experimental determined value.

3.3. Compression creep behavior of coatings

3.3.1. Overview

An overview of all creep tests conducted, the apparent steady-state strain rate, the total plastic strain that occurred during the creep test, and the number of replicates is given in Table 4. The apparent steady-state strain rates of each specimen were calculated from the slope of the linear portion of the creep data. All stand-alone coating specimens showed typical creep behavior with an initial elastic strain on loading, followed by a transient, high-strain rate region, and an apparent linear, steady-state region. At a test temperature of ≥1100 °C and a stress of ≥60 MPa, YSZ samples barreled during creep testing. YSZ samples tested at 1200 °C and 80 MPa barreled and then failed within the 5 h test (see the top plot in Fig. 5), exhibiting tertiary creep. Barreling in the YSZ specimens indicates a significant amount of friction between the load cell platens and the ends of the stand-alone coating.[30] The effect of this friction on the present experimental data has not been determined. Barreling was not visually observed in composite or mullite specimens under the conditions investigated.

As shown in Fig. 5, a comparison of the behavior of the coatings under 40, 60, and 80 MPa at 1200 °C, increasing the applied stress on the coatings increased the total amount the specimens crept and the apparent steady-state creep rates in all coating types. For example, YSZ coatings tested at 1200 °C exhibited a total creep strain of ∼2.5, ∼4.0, and ∼6.3% (failed prior to 5 h) under stresses of 40, 60, and 80 MPa. From the results on YSZ,

Table 4
Overview of all creep tests on YSZ, composite, and mullite samples

Specimen	Stress (MPa)	Temperature (°C)	Apparent steady-state strain rate in compression (s^{-1})	Total compressive creep strain (%)	Replicates
YSZ	40	1000	$5.9 \times 10^{-8} \pm 1.6 \times 10^{-8}$	0.34 ± 0.09	4
YSZ	40	1050	7.5×10^{-8}	0.39	1
YSZ	40	1100	1.6×10^{-7}	0.80	1
YSZ	40	1150	3.3×10^{-7}	1.36	1
YSZ	40	1200	$7.2 \times 10^{-7} \pm 3.0 \times 10^{-8}$	2.46 ± 0.10	3
YSZ	60	1000	$6.2 \times 10^{-8} \pm 5.5 \times 10^{-9}$	0.33 ± 0.01	2
YSZ	60	1050	1.1×10^{-7}	0.57	1
YSZ	60	1100	2.1×10^{-7}	0.98	1
YSZ	60	1150	5.5×10^{-7}	1.98	1
YSZ	60	1200	$1.6 \times 10^{-6} \pm 4.4 \times 10^{-7}$	4.00	2
YSZ	80	1000	$1.0 \times 10^{-7} \pm 5.0 \times 10^{-9}$	0.58 ± 0.00	2
YSZ	80	1050	1.4×10^{-7}	0.70	1
YSZ	80	1100	3.3×10^{-7}	1.50	1
YSZ	80	1150	8.2×10^{-7}	2.74	1
YSZ	80	1200	$3.6 \times 10^{-6} \pm 3.5 \times 10^{-7}$	6.25 ± 0.08[a]	2
Composite	40	1000	$3.0 \times 10^{-8} \pm 9.2 \times 10^{-9}$	0.21 ± 0.05	7
Composite	40	1100	1.0×10^{-7}	0.60	1
Composite	40	1200	$2.5 \times 10^{-7} \pm 2.7 \times 10^{-8}$	1.27 ± 0.13	3
Composite	60	1000	$4.9 \times 10^{-8} \pm 1.2 \times 10^{-8}$	0.28 ± 0.06	2
Composite	60	1100	1.4×10^{-7}	0.75	1
Composite	60	1200	3.7×10^{-7}	1.61	1
Composite	80	1000	$5.5 \times 10^{-8} \pm 1.7 \times 10^{-8}$	0.33 ± 0.13	3
Composite	80	1100	$2.0 \times 10^{-7} \pm 4.5 \times 10^{-8}$	1.02 ± 0.23	3
Composite	80	1200	6.7×10^{-7}	2.33	1
Mullite	40	1000	$1.5 \times 10^{-8} \pm 2.5 \times 10^{-9}$	0.10 ± 0.03	3
Mullite	40	1100	4.0×10^{-8}	0.24	1
Mullite	40	1200	$7.0 \times 10^{-8} \pm 3.0 \times 10^{-9}$	0.41 ± 0.02	3
Mullite	60	1000	1.5×10^{-8}	0.12	1
Mullite	60	1100	4.6×10^{-8}	0.24	1
Mullite	60	1200	$1.1 \times 10^{-7} \pm 1.4 \times 10^{-8}$	0.58 ± 0.08	2
Mullite	80	1000	2.3×10^{-8}	0.11	1
Mullite	80	1100	6.2×10^{-8}	0.33	1
Mullite	80	1200	1.4×10^{-7}	0.76	1

[a] Extensive barreling noted in this sample.

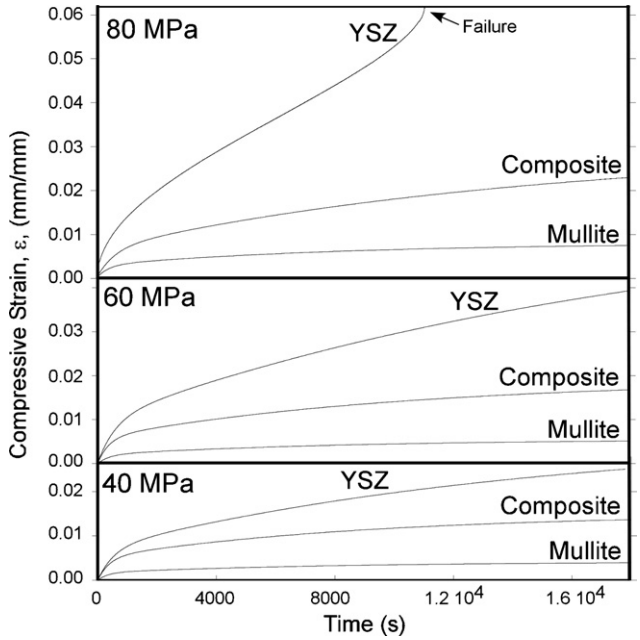

Fig. 5. Representative comparison of the creep behavior of YSZ, mullite, and composite coatings at 1200 °C under 40, 60, and 80 MPa. The behavior of the composite was consistently in between that of the mullite and YSZ coatings. YSZ coatings failed under 80 MPa and barreled under 60 MPa loads at this temperature. Note that the elastic response for each sample was subtracted from this data.

the threshold strain where barreling begins to occur is ∼4%. Tests on mullite at 1200 °C and compressive stresses of 40, 60, and 80 MPa conditions demonstrated a total strain of ∼0.4, ∼0.6 and ∼0.8%, respectively. As is observed in Fig. 5, the composite coating exhibited total creep deformation behavior that was more similar to mullite than YSZ. This finding was most evident in the composite coatings tested at 1200 °C and 80 MPa, where only ∼2.3% deformation was measured during creep and no barreling was visually observed.

YSZ tested at 1200 °C and stresses of 40, 60, and 80 MPa exhibited apparent steady-state strain rates of $\sim 7.2 \times 10^{-7}$, $\sim 1.6 \times 10^{-6}$, and $\sim 3.6 \times 10^{-6}\ s^{-1}$, respectively. Barreling would contribute to the latter two strain rates, resulting in higher rates than if only the YSZ was contributing to deformation. At the same test temperature, mullite samples demonstrated strain rates of $\sim 7.0 \times 10^{-8}$, $\sim 1.1 \times 10^{-7}$, and $\sim 1.4 \times 10^{-7}\ s^{-1}$ at applied stresses of 40, 60, and 80 MPa. These values were typically one order of magnitude less that those observed in the YSZ samples, and they showed no evidence of barreling. Composite creep rates were generally closer to mullite creep rates than YSZ. For example, a composite specimen crept at 1200 °C and 80 MPa displayed a creep rate of $6.7 \times 10^{-7}\ s^{-1}$.

Increasing test temperatures resulted in a greater amount of creep strain and higher creep rates for all of the coating materials. YSZ coatings tested at 60 MPa and 1000, 1100, and 1200 °C exhibited total deformations of ∼0.33, ∼1.00, and ∼4.00%, respectively. Mullite coatings tested under the same stress and temperatures exhibited total deformations of ∼0.12, ∼0.24, and ∼0.58%, respectively. The creep strain observed in a composite sample at 1200 °C and 60 MPa was ∼1.60%. Steady-state creep rates increased nearly two orders of magnitude from $\sim 10^{-8}$ to $\sim 10^{-6}\ s^{-1}$ from 1000 to 1200 °C in YSZ coatings tested at 60 MPa, but no more than one order of magnitude, from 10^{-8} to $10^{-7}\ s^{-1}$, in mullite and composite coatings tested under the same conditions. It is important to realize that these results have not been normalized to account for differences in porosity between coating types. Thus, the greater porosity in the composite specimens was not detrimental to the creep behavior when compared to the less porous YSZ specimens.

It is valuable to compare sintering rates of dense YSZ and mullite samples to the porous coatings investigated presently. Sudhir and Chokshi[31] investigated the compression creep characteristics of dense 8 mol% yttria-stabilized cubic zirconia. At 1400 °C, the lowest temperature studied, and a compressive stress of 80 MPa, they observed a steady-state creep rate of $4 \times 10^{-7}\ s^{-1}$. As noted in Table 4, YSZ specimens tested at 1200 °C and 80 MPa demonstrated a steady-state creep rate of $3.6 \times 10^{-6}\ s^{-1}$. While slight barreling of these samples may have artificially increased their strain rate, these coatings demonstrated comparable strain rates to dense YSZ but were tested at a 200 °C lower temperature. The primary mechanism of creep in the stress and temperature ranges of interest for the dense specimens studied by Sudhir and Chokshi was identified as vacancy flow along grain boundaries (i.e. Coble creep).

In a study by Torrecillas et al.[32], dense mullite crept in compression at 1200 °C and 80 MPa demonstrated a steady-state creep rate of $2.0 \times 10^{-9}\ s^{-1}$. In the present study, mullite tested at 1200 °C and 80 MPa displayed a steady-state creep rate in compression of $1.4 \times 10^{-7}\ s^{-1}$, substantially greater that of the dense mullite. The primary mechanism of creep in the range of temperatures and stresses measured currently was attributed by Torrecillas et al.[32] to accommodated grain boundary sliding assisted by diffusion.

Some creep testing has been performed on mullite/zirconia composites, however, the test conditions and starting microstructures are vastly different than those evaluated in this study. For example, Descamps et al.[33] investigated the creep response of 70 vol.% mullite/30 vol.% zirconia composites in bending (tensile creep was reported) on samples prepared by reaction sintering of zirconium silicate and alumina using titania and magnesia additives. At 1200 °C and a tensile stress of 80 MPa, creep rates of 3×10^{-8} to $3 \times 10^{-7}\ s^{-1}$ were measured. These were similar to those observed presently. In addition to the different stress state in the materials (i.e. tension creep in the cited study and compression creep presently), the microstructures of these materials were vastly different than those studied presently, with 1–5 μm diameter equiaxed zirconia grains in a mullite matrix observed.

3.3.2. Mechanisms of deformation

The creep rates observed for plasma-sprayed YSZ and mullite coatings were at least two orders of magnitude greater than those for dense specimens of the same material tested at similar conditions. These results suggest that the creep mechanisms governing the deformation behavior of dense YSZ or mullite do not significantly contribute to either of these plasma-sprayed materials.

Stress relaxation experiments on plasma-sprayed YSZ cylinders[12] have revealed deformation mechanisms that are likely similar to those experienced during creep and may provide insight into the current data. YSZ has been shown to relax uniaxial compressive stresses in two stages. In stage I of relaxation, stress is relieved by the initiation and growth of cracks parallel to the applied load, the healing of cracks perpendicular to the applied load, and the sliding and mechanical compaction of lamellae. In stage II, relaxation of the applied stress occurs at a slower rate. Research indicates that stage II relaxation is likely due to stress-assisted densification of the coating and possibly the intrinsic deformation properties of the material being testing.[12,13] However, the current creep data suggest that for test times considered currently (~5 h) that only stress-assisted densification is responsible for deformation. This result has been noted by Thurn et al.[27], where they observed a 6% reduction in open porosity (from 22 to 16%) as a result of a compressive creep strain of 1%. In the current data set, an approximate 1% reduction in total porosity was noted in the YSZ coating after a 5 h creep test at 80 MPa and 1200 °C. Neither the mullite or YSZ/mullite samples showed a change in porosity as a result of the creep test. However, the transformation from amorphous to crystalline mullite during heating through ~970 °C may complicate the measurement by affecting the density of the coating.

Stress exponents were calculated for the individual data sets by plotting apparent steady-state strain versus stress (not shown). Within the resolution of the data, stress exponents for the YSZ, mullite, and composite tubes were equal to 1 for test temperatures of 1000 and 1100 °C. At 1200 °C, the stress exponent for the YSZ sample was 2.3, while for the mullite and YSZ/mullite composite samples it was 1. The higher stress exponent for the YSZ at 1200 °C is likely due to contributions from sample barreling. A stress exponent of 1 corresponds to that expected for either diffusion or grain boundary sliding accommodated by diffusion.[34] Because densification is controlled by diffusion of atomic species in the range of pressures and temperatures investigated, the stress exponent would also be expected to be 1. Thus, the measured stress exponents in the current data set are consistent with the proposed mechanism of deformation.

3.3.3. Creep activation energies for the coatings investigated

The apparent steady-state strain rates of each specimen were used to determine the activation energies for creep in each coating type. As shown in Fig. 6, activation energies were determined by measuring the slope of a line fit through data points on a plot of $\ln(\dot{\varepsilon})$ versus $1/T$.

Two activation energies were observed in the $\ln(\dot{\varepsilon})$ versus $1/T$ behavior of YSZ for each applied stress. For an applied stress of 80 MPa the activation energy was 410 ± 40 kJ/mol between 1100 and 1200 °C, and 164 ± 40 kJ/mol between 1100 and 1000 °C. As shown in Fig. 6, similar behavior was observed for creep tests conducted at 40 and 60 MPa. Two possible reasons exist for this behavior. As stated previously, barreling was observed at test temperatures ≥1100 °C and for stresses ≥60 MPa. When coatings barrel, significant bending stresses would increase the strain rate observed during individual tests. The increase in strain rate associated with barreling would produce an apparent increase in activation energy and likely contribute to the activation energy differences observed presently, particularly in the 60 and 80 MPa data shown in Fig. 6 for YSZ. However, no barreling was observed in the data collected at 40 MPa, yet the activation energy showed a similar increase from 1000 to 1200 °C as the samples that barreled. Erk et al.[35] have shown a transition in the mass transport phenomena in plasma-sprayed 7 wt.% YSZ coatings from surface diffusion dominant at 1000 °C to grain boundary diffusion dominant at temperatures of 1200 °C and above. At 1100 °C, both grain boundary and surface diffusion appear to be competing. Thus, the two values of activation energy observed for YSZ in Fig. 6 in the 1000 to 1100 °C and 1100 to 1200 °C temperature ranges may be due to both barreling and a change in the mass transport mechanism during densification.

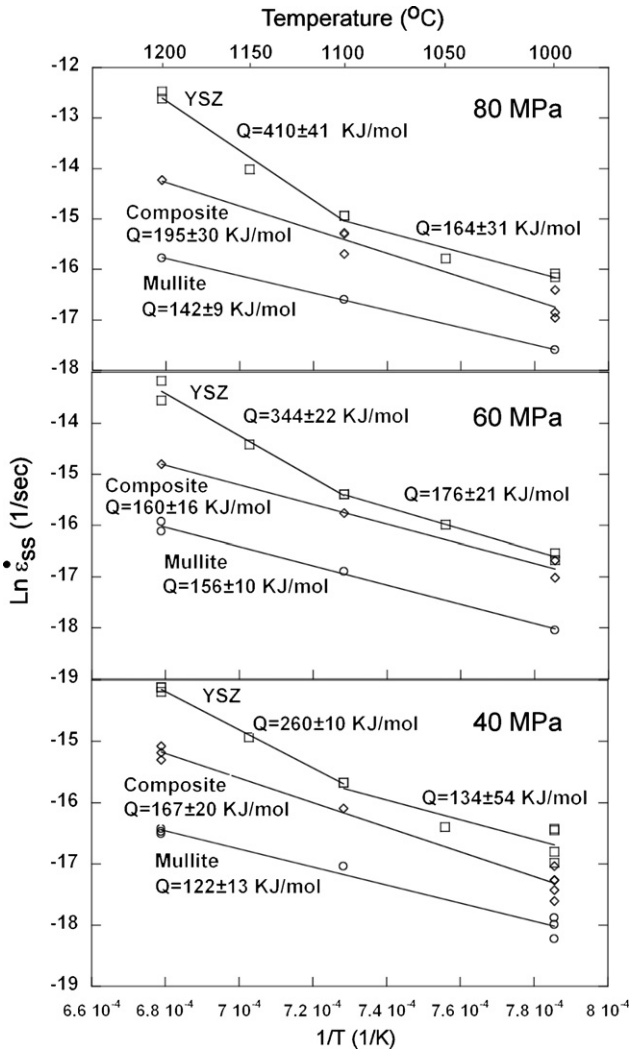

Fig. 6. Plot of natural log of steady-state strain rate vs. one over absolute temperature of YSZ, mullite, and the YSZ/mullite composite coatings tested under constant load.

Published creep studies on plasma-sprayed YSZ are limited.[25,27,36–38] Thurn et al.[27] measured an activation energy of 114 kJ/mol for air-plasma-sprayed YSZ tested in compression

using a set-up similar to that used in this study. The temperature range varied from 900 to 1100 °C, and applied stresses ranged from 20 to 80 MPa. The reported activation energy by Thurn et al. is similar to that reported here for temperatures ≤1100 °C, particularly for the data collected at 40 MPa.

The activation energies for mullite ranged from 122 to 156 kJ/mol between 1000 and 1200 °C, essentially independent of the applied stress. Within the error of the measurements, the same conclusion can be made regarding the activation energies of the YSZ/mullite composite samples. It should be noted that no change in the slope of the $\ln(\dot{\varepsilon})$ versus $1/T$ data was observed in the composite creep data, suggesting that the deformation mechanism(s) remained unchanged from 1000 to 1200 °C and that the creep behavior of YSZ/mullite composites was dominated by the mullite phase.

No prior work citing creep studies of plasma-sprayed mullite were found. Compression creep activation energies reported in the literature for dense mullite prepared using conventional powder processing techniques have typically been more than twice those measured presently. Torrecillas et al.[32] measured an activation energy for compression loaded mullite of 410 kJ/mol between 1100 and 1300 °C. This energy was independent of stresses investigated between 30 and 70 MPa, as was the case for the samples tested presently. The difference in activation energy between dense and plasma-sprayed mullite is attributed to the fact that stress-assisted densification, not grain boundary sliding assisted by diffusion, is controlling the deformation of the porous coatings.

3.3.4. Implications of mullite properties on TBC performance

In the present study, the continuous mullite phase clearly dominates the steady-state creep rate in the composite samples. However, by forming two-phase coatings of a low thermal conductivity phase (i.e. YSZ) and a higher thermal conductivity phase (i.e. mullite), a decrease in the thermal resistance of the topcoat does occur. In data measured for as-sprayed mullite/YSZ composite coatings similar in composition to those studied here, the thermal conductivity was 1.3 W/m/K at 1000 °C.[39] For similar test conditions, a plasma-sprayed YSZ sample demonstrated a thermal conductivity of 0.8 W/m/K. Both of these values were measured using the laser flash technique. Thus, it is clear that composite mullite/YSZ topcoat would not be as effective at protecting the underlying substrate as a pure YSZ topcoat.

As presented in Table 3, the CTE of the mullite/YSZ coating is ∼40% less than the YSZ-only coating. Because the CTE of the YSZ more nearly matches that of the underlying metallic structure, the development of thermally generated stresses between the mullite/YSZ coating and the underlying structure would be greater than for the YSZ-only coating. However, it must be remembered that the coating investigated here represents a first effort to blend mullite and YSZ into a useful coating system. Grading the amount of the mullite through the thickness of the coating could result in optimal system performance. By making the outer layer rich in the mullite phase, creep of this region can be reduced because of the intrinsic resistance of mullite to stress-assisted densification. This reduction in deformation should lower the amount of through thickness cracks that form after extended service at high temperatures. By reducing the amount of mullite in the interior part of the coating, the low thermal conductivity of the YSZ could be maintained, and the inner YSZ-rich layer would also preserve the CTE necessary to match that of the metallic structure.

4. Summary

The thermal expansion and creep behavior of stand-alone coatings of 7 wt.% Y_2O_3–ZrO_2, mullite, and a 46:54 volume ratio composite of YSZ:mullite were characterized. Cylindrical coatings were subject to uniaxial compression creep tests under stresses ranging from 40 to 80 MPa for 5 h at temperatures between 1000 and 1200 °C. The primary deformation mechanism in coatings made from all three materials was densification of the porous coating. Overall, the YSZ/mullite composite showed improved creep resistance over YSZ-only coatings and should be investigated further for its possible use in thermal barrier coating systems.

Acknowledgements

This work was supported by the National Science Foundation through DMR-0134286 and by a donation from Praxair Surface Technologies Inc.

References

1. Clarke, D. R. and Levi, C. G., Materials design for the next generation thermal barrier coatings. *Annu. Rev. Mater. Res.*, 2003, **33**, 383–417.
2. Ramaswamy, P., Seetheramu, S., Varma, K. B. R., Raman, N. and Rao, K. J., Thermomechanical fatigue characterization of ZrO_2 and mullite thermal barrier coatings on diesel engine components: effect of coatings on engine performance. *Proc. Inst. Mech. Eng. Part C J. Mech. Sci.*, 2000, **214**(5), 729–742.
3. Miller, R. A., Levine, S. R. and Hodge, P. E., Thermal barrier coatings for superalloys. In *Proceedings Fourth International Symposium on Superalloys*. Seven Springs, PA, September 21–25. American Society for Metals, Metals Park, OH, 1980, pp. 473–480.
4. Beele, W., Marijnissen, G. and Van Lieshout, A., The evolution of thermal barrier coatings—status and upcoming solutions for today's key issues. *Surf. Coat. Technol.*, 1999, **120**, 61–67.
5. Miller, R. A., Current status of thermal barrier coatings—an overview. *Surf. Coat. Technol.*, 1987, **30**, 1–11.
6. McPherson, R., A review of microstructure and properties of plasma sprayed ceramic coatings. *Surf. Coat. Technol.*, 1989, **39/40**, 173–181.
7. McPherson, R., The relationship between mechanism of formation, microstructure and properties of plasma-sprayed coatings. *Thin Solid Films*, 1981, **83**, 297–310.
8. Miller, R. A. and Lowell, C. E., Failure mechanisms of thermal barrier coatings exposed to elevated temperatures. *Thin Solid Films*, 1982, **95**, 265–273.
9. Miller, R. A., Thermal barrier coatings for aircraft engines—history and direction. *J. Therm. Spray Technol.*, 1997, **6**(1), 35–42.
10. Ilavsky, J. and Stalick, J. K., Phase composition and its changes during annealing of plasma-sprayed YSZ. *Surf. Coat. Technol.*, 2000, **127**, 120–129.
11. Kokini, K., Banerjee, A. and Taylor, T. A., Thermal fracture of interfaces in pre-cracked thermal barrier coatings. *Mater. Sci. Eng. A*, 2002, **323**, 70–82.
12. Dickinson, G. R., Petorak, C. A., Bowman, K. and Trice, R. W., Stress relaxation of compression loaded plasma-sprayed 7 wt% Y_2O_3–ZrO_2 stand-alone coatings. *J. Am. Ceram. Soc.*, 2005, **88**(8), 2202–2208.

13. Petorak, C. A., *High temperature mechanical behavior of plasma-sprayed 7 wt.% yttria-stabilized zirconia stand-alone coatings*. Thesis. Purdue University, June 2005.
14. Rejda, E. F., Socie, D. F. and Itoh, T., Deformation behavior of plasma-sprayed thick thermal barrier coatings. *Surf. Coat. Technol.*, 1999, **113**, 218–226.
15. Kokini, K., Takeuchi, Y. R. and Choules, B. D., Surface thermal cracking of thermal barrier coatings owing to stress relaxation: zirconia vs mullite. *Surf. Coat. Technol.*, 1996, **82**, 77–82.
16. Choules, B. D., Kokini, K. and Taylor, T. A., Thermal fracture of ceramic thermal barrier coatings under heat flux with time-dependent behavior. Part 1. Experimental results. *Mater. Sci. Eng. A*, 2001, **299**, 296–304.
17. Kingery, W. D., Bowen, H. K. and Uhlmann, D. R., *Introduction to Ceramics* (*2nd ed.*). Wiley, New York, 1976, p. 240, 595, 304 and 642.
18. Lessing, P. A., Gordon, R. S. and Mazdiyasni, K. S., Creep of polycrystalline mullite. *J. Am. Ceram. Soc.*, 1975, **58**(3–4), 149.
19. Dokko, P. C., Pask, J. A. and Mazdiyasni, K. S., High-temperature mechanical properties of mullite under compression. *J. Am. Ceram. Soc.*, 1977, **60**(3–4), 150–155.
20. Yoon, C. K. and Chen, I. W., Superplastic flow of two-phase ceramics containing rigid inclusions—zirconia/mullite composites. *J. Am. Ceram. Soc.*, 1990, **73**(6), 1555–1565.
21. Friel, J. J., *Practical Guide to Image Analysis*. ASM International, Materials Park, OH, 2000, p. 19.
22. Standard test method for water absorption, bulk density, apparent porosity, and apparent specific gravity of fired whiteware products, ASTM Standard C 373-72. In *ASTM Annual Book of Standards*. American Society for Testing and Materials, West Conshohocken, PA, 1982.
23. Lee, W. E. and Rainforth, W. M., *Ceramic Microstructures: Property Control by Processing*. Chapman and Hall, New York, 1994, p. 310.
24. Wachtman, J. B., *Mechanical Properties of Ceramics*. Wiley, New York, 1996, p. 392.
25. Echsler, H., Renusch, D. and Schutze, M., Mechanical behavior of as sprayed and sintered air plasma sprayed partially stabilized zirconia. *Mater. Sci. Technol.*, 2004, **20**, 869–876.
26. Bowman, K., *Mechanical Behavior of Materials*. John Wiley and Sons, Inc., 2004.
27. Thurn, G., Schneider, G. A. and Aldinger, F., High-temperature deformation of plasma-sprayed ZrO_2 thermal barrier coatings. *Mater. Sci. Eng. A*, 1997, **233**, 176–182.
28. Lee, K. N., Miller, R. A. and Jacobson, N. S., New generation of plasma-sprayed mullite coatings on silicon carbide. *J. Am. Ceram. Soc.*, 1995, **78**(3), 705–710.
29. Schneider, H., Okada, K. and Pask, J. A., *Mullite and Mullite Ceramics*. John Wiley & Sons, New York, 1994, pp. 224–225.
30. Debschutz, K. D., Caspers, B., Schneider, G. A. and Petzow, G., Critical evaluation of the compression test. *J. Am. Ceram. Soc.*, 1993, **76**(10), 2468–2474.
31. Sudhir, B. and Chokshi, A., Compression creep characteristics of 8-mol%-yttria-stabilized cubic-zirconia. *J. Am. Ceram. Soc.*, 2001, **84**(11), 2625–2632.
32. Torrecillas, R., Calderon, J. M., Moya, J. S., Reece, M. J., Davies, C. K. L., Olagnon, C. and Fantozzi, G., Suitability of mullite for high temperature applications. *J. Eur. Ceram. Soc.*, 1999, **19**, 2519–2527.
33. Descamps, P., Sakaguchi, S., Poorteman, M. and Cambier, F., High-temperature characterization of reaction sintered mullite–zirconia composites. *J. Am. Ceram. Soc.*, 1991, **74**(10), 2476–2481.
34. Green, D., An Introduction to the Mechanical Properties Of Ceramics. *Cambridge Solid State Science Series*., 1998, p. 200.
35. Erk, K. A., Deschaseaux, C. and Trice, R. W., Grain boundary grooving of plasma-sprayed yttria-stabilized zirconia thermal barrier coatings. *J. Am. Ceram. Soc.*, 2006, **89**(5), 1673–1678.
36. Ahrens, M., Lampenscherf, S., Vassen, R. and Stover, D., Sintering and creep responses in plasma-sprayed thermal barrier coatings. *J. Therm. Spray Technol.*, 2004, **13**(3).
37. Zhu, D. and Miller, R., Sintering and creep behavior of plasma-sprayed zirconia- and hafnia-based thermal barrier coatings. *Surf. Coat. Technol.*, 1998, **108–109**, 114–120.
38. Zhu, D. and Miller, R., *Determination of Creep Behavior of Thermal Barrier Coatings Under Laser Imposed Temperature and Stress Gradients, NASA Technical Memorandum 113169*. Lewis Research Center, 1997.
39. Private conversation with Dr. Thomas Taylor.